SCIENTIFIC REPORTS

OPEN

WS_2 mode-locked ultrafast fiber laser

Dong Mao, Yadong Wang, Chaojie Ma, Lei Han, Biqiang Jiang, Xuetao Gan, Shijia Hua, Wending Zhang, Ting Mei & Jianlin Zhao

Key Laboratory of Space Applied Physics and Chemistry, Ministry of Education; and Shaanxi Key Laboratory of Optical Information Technology, School of Science, Northwestern Polytechnical University, Xi'an 710072, China.

SUBJECT AREAS:
FIBRE LASERS
TWO-DIMENSIONAL MATERIALS

Received
7 October 2014

Accepted
2 January 2015

Published
22 January 2015

Correspondence and requests for materials should be addressed to D.M. (maodong@nwpu.edu.cn)

Graphene-like two dimensional materials, such as WS_2 and MoS_2, are highly anisotropic layered compounds that have attracted growing interest from basic research to practical applications. Similar with MoS_2, few-layer WS_2 has remarkable physical properties. Here, we demonstrate for the first time that WS_2 nanosheets exhibit ultrafast nonlinear saturable absorption property and high optical damage threshold. Soliton mode-locking operations are achieved separately in an erbium-doped fiber laser using two types of WS_2-based saturable absorbers, one of which is fabricated by depositing WS_2 nanosheets on a D-shaped fiber, while the other is synthesized by mixing WS_2 solution with polyvinyl alcohol, and then evaporating them on a substrate. At the maximum pump power of 600 mW, two saturable absorbers can work stably at mode-locking state without damage, indicating that few-layer WS_2 is a promising high-power flexible saturable absorber for ultrafast optics. Numerous applications may benefit from the ultrafast nonlinear features of WS_2 nanosheets, such as high-power pulsed laser, materials processing, and frequency comb spectroscopy.

Since the single- or few-layer graphene was fabricated by using mechanical exfoliation method, it has been in-depth investigated and widely used in various fields, including photon detection, graphene plasmonics, ultrafast optics, and quantum electrodynamics[1–5]. Research on graphene also opened up a door to new two-dimensional (2D) nanomaterials in which strong covalent bonds in layers and weak van der Waals interaction between layers exist. Following the similar approach on graphene study, researchers have developed various graphene analogues of layered inorganic materials comprising stacked atomic or molecular layers, such as topological insulator[6–8], molybdenum disulfide (MoS_2)[9], tungsten disulphide (WS_2)[10], etc. Among them, topological insulator nanosheets are proven to exhibit saturable absorption property[7,8], in which the optical absorbance decreases with the enhancement of the incident laser intensity and becomes saturated above a certain threshold. Graphene-[11,12] and topological insulator-[7,8,13] based saturable absorbers (SAs) possess inherent features of broad response as well as high flexibility, and have been broadly used in Q-switching and mode-locking lasers. Bonaccorso *et al.* summarized graphene and other 2D crystals based ultrafast photonics, from solution processing, fabrication of SAs, to their applications in ultrafast lasers[14].

The bulk MoS_2 and WS_2 are indirect semiconductors, which consist of hexagonal layers of metal atoms sandwiched between two layers of chalcogen atomsare[15]. Like graphene, these layered materials could be exfoliated into thin film to explore their exotic features for practical applications. Various methods, such as mechanical exfoliation[16], liquid exfoliation[17], hydrothermal intercalation/exfoliation[18], chemical vapor deposition[19], as well as two-step expansion and intercalation[20] have been developed to synthesize few-layer MoS_2 and WS_2 nanosheets. Compared with their bulk counterparts, the monolayer MoS_2 and WS_2 possess a direct bandgap and show significant improvement in photoluminescence quantum efficiency attributing to the 2D confinement of electron motion and the absence of interlayer perturbation[9,21]. Recently, a great deal of research interest is focused on the nonlinear absorption property of MoS_2 nanosheets[22–27]. For example, K. Wang *et al.* demonstrated that MoS_2 nanosheets exhibited significant saturable absorption with a relaxation of 30 fs and had better saturable absorption than that of graphene for femtosecond pulse at 800 nm[22]. They concluded that the ultrafast saturable absorption of the MoS_2 nanosheets originated from one-photon induced free-carrier absorption. After that, S. Wang *et al.* showed that when the ratio between Mo and S ions was increased from 2 to 2.09, the MoS_2 bandgap can be reduced from 1.08 to 0.08 eV (corresponding to an absorption wavelength of 15.4 μm). By introducing suitable defects, they have realized a broadband MoS_2 SA that has been used in Q-switched lasers operating at 1.06, 1.42, and 2.1 μm[23]. H. Zhang *et al.* systematically investigated the nonlinearity of MoS_2 nanosheets using open-aperture Z-scan and balanced-detector measurement techniques, and demonstrated a yttrium-doped fiber laser passively mode locked with a MoS_2 SA[24]. They infer that the broadband absorption property may arise from the coexistence of semiconducting and metallic states in the layered 2D materials. Currently, H. Liu *et al.* and H.

Xia *et al.* have realized femtosecond and picosecond pulses in erbium-doped fiber (EDF) lasers mode locked by MoS_2 SAs, respectively[25,26]. R. Khazaeizhad *et al.* have realized passive mode locking in anomalous- and normal-dispersion regimes using a multilayer MoS_2 thin film coated on D-shaped fiber[27]. The aforementioned investigations are mainly focused on MoS_2, while that of WS_2 are not stressed and its applications remain untapped. Whether WS_2 exhibits saturable absorption property as that of graphene or MoS_2? How to fabricate WS_2-based mode locker to realize ultrafast pulse emission? In this paper, we focus on these important issues.

Here, we demonstrate that WS_2 nanosheets exhibit nonlinear saturable absorption property and ultra-high optical damage threshold. Soliton mode locking is achieved separately in a fiber laser by using two different types of WS_2 SAs, one of which is fabricated by depositing WS_2 on D-shaped fiber, while the other is synthesized by mixing WS_2 solution with polyvinyl alcohol (PVA), and then evaporating them on a substrate. At the maximum pump power of 600 mW, two SAs can work stably without damage in the mode-locked fiber laser, indicating that WS_2-based SAs possess ultra-high damage threshold. Our results demonstrate that WS_2 nanosheets exhibit saturable absorption property at 1.55 μm and can work as a high-power mode locker for ultrafast fiber lasers.

Results

Preparation and characterization of WS_2-based SAs. The liquid exfoliation is a simple and effective method for preparing high-quality 2D nanostructures[17,22]. In this experiment, the solvent for dispersing WS_2 flakes is fabricated by mixing ethanol and water at the volume ratio of 35 : 75. The initial dispersions are treated for 120 min by a high-power ultrasonic cleaner. After sonication, the

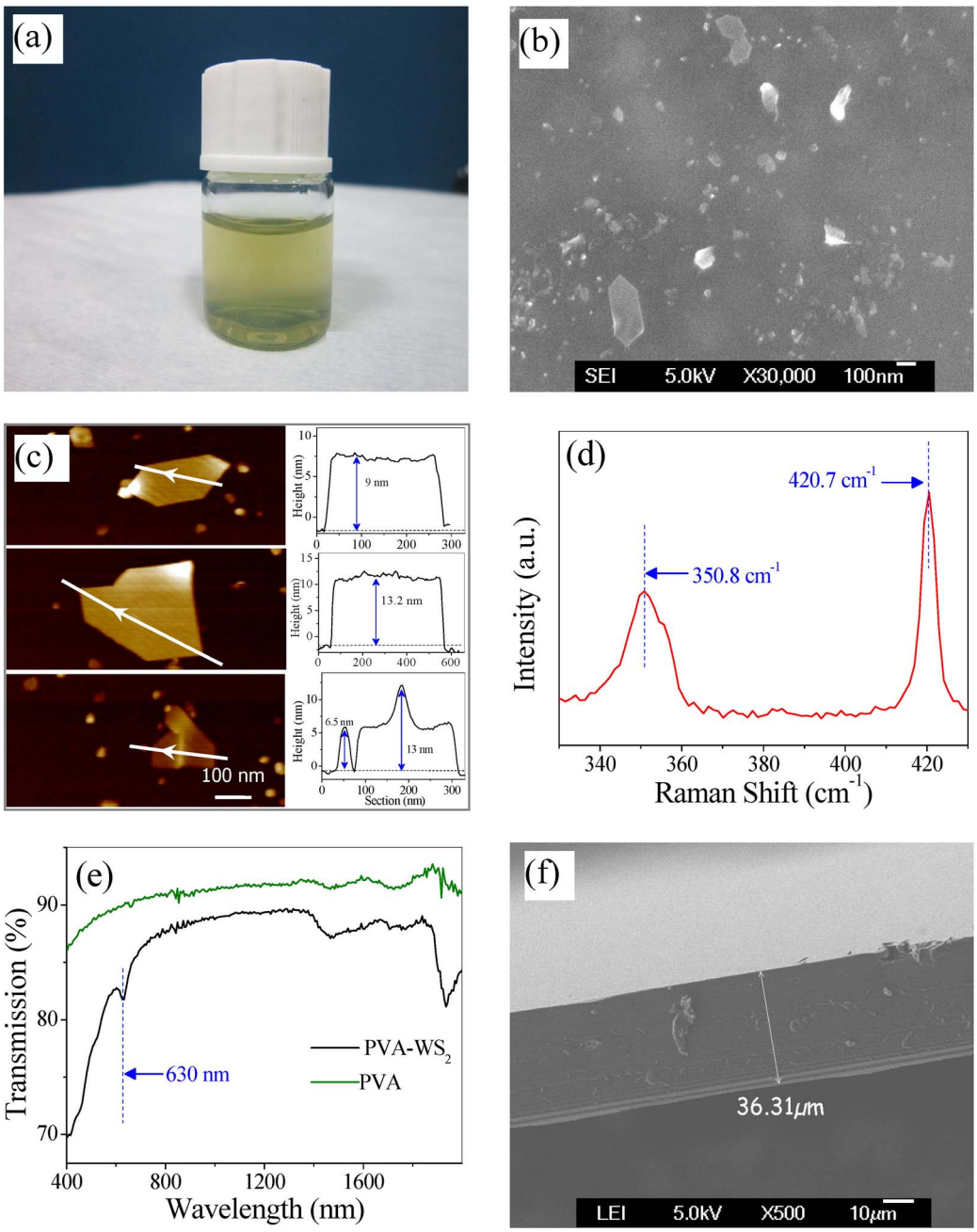

Figure 1 | (a) Image of WS_2 dispersion; (b) SEM image, and (c) AFM image, (d) Raman spectrum of WS_2 nanosheets; (e) linear transmission spectrum of the WS_2-PVA film in comparison with pure PVA-film, (f) side profile of WS_2-PVA film. The thickness of the film is measured as 36.31 μm.

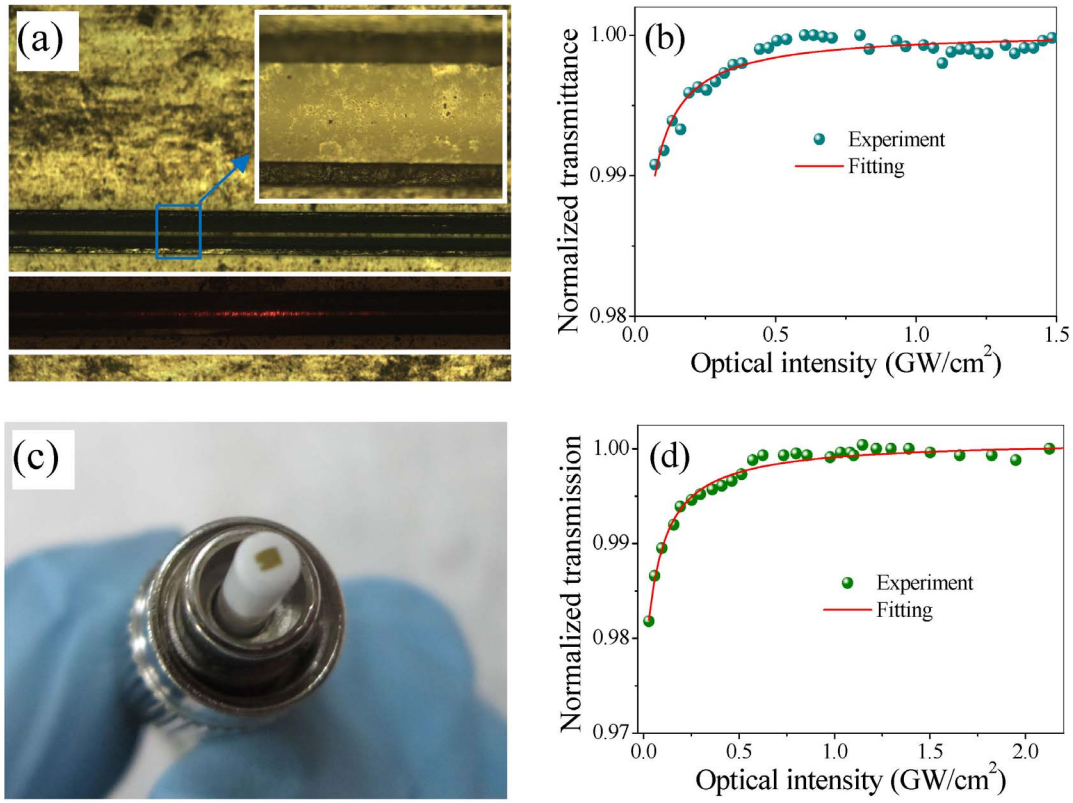

Figure 2 | (a) Photograph of the D-shaped fiber coated with WS_2, the middle and down images show the D-shaped fiber before and after injecting 632.8 nm laser, and the upward image shows the zoom-in image of D-shaped fiber; (b) nonlinear transmission of D-shaped fiber WS_2 SA; (c) WS_2-PVA film attached on the facet of fiber connector; (d) nonlinear transmission of WS_2-PVA film.

dispersions are allowed to settle for several hours. To remove large agglomeration, the WS_2 dispersions are centrifuged at 3000 rpm for 30 min, and the upper supernatant is collected. The concentration of WS_2 nanosheets in the solvent is ~0.1 mg/ml. As shown in Fig. 1(a), the typical dispersions show a faint yellow-green color, and are stable over tens of days. Figure 1(b) shows the scanning electron microscopy (SEM) image of WS_2 nanosheets on silicon slice. The width and length of WS_2 nanosheets are in the range of 50 to 500 nm. By using an atomic force microscope (AFM), we find that the thickness of nanosheets ranges from 2 to 20 nm. Figure 1(c) shows three typical AFM images of WS_2 nanosheets. The deposited WS_2 nanosheets are further characterized by Raman spectroscopy using Ar laser at 514 nm, as depicted in Fig. 1(d). The characteristic bands at 350.8 and 420.7 cm^{-1} on the Raman spectrum are assigned to the in-plane (E_{2g}) and out-of-plane (A_{1g}) vibrational modes of WS_2, in agreement with the earlier findings[28]. Figure 1(e) plots the linear transmission spectrum of the WS_2-PVA film in comparison with pure PVA film, which is measured by a spectrometer (Hitachi UV4100). The dip at 630 nm on the transmission spectrum could be attributed to the direct gap transition[17]. The side profile of WS_2-PVA film is measured with a SEM, and the thickness of the film is given as 36.31 μm, as shown in Fig. 1(f). Analysis of SEM profile, AFM image, Raman spectrum, and linear transmission suggests the presence of WS_2 nanosheets in the sample.

In our experiment, two different WS_2 SAs are used to achieve passive mode locking. The first SA is realized by nonlinear interaction of WS_2 nanosheets with the evanescent field of light in a D-shaped fiber. Here, the D-shaped fiber is prepared by polishing a single-mode fiber (SMF) after holding the fiber with an arcuate block. During polishing, the insertion loss that indicates the space between the fiber core and the polished surface is monitored by an optical power meter. The WS_2 nanosheets are adhered on the D-shaped fiber by using optical deposition method. First, the WS_2 solution is dropped on a D-shaped fiber that is fixed at a quartz plate. Then, a 10 mW continues wave centered at 1.55 μm is coupled into the D-shaped fiber and the optical deposition process starts. An optical power meter is used to evaluate the deposition depth real-timely. This approach is similar to the carbon nanotube mode locker via evanescent field interaction in D-shaped fibers[29] or topological insulator mode locker based on tapered fibers[8].

The microscope images of the D-shaped fiber coated with WS_2 are shown in Fig. 2(a). The upward inset and middle images show the D-shaped fiber at a magnification of 200-fold and 20-fold, respectively, while the downward inset shows the evanescent field of light in the D-shaped fiber using a 632.8 nm He-Ne laser. The insertion loss of the integrated D-shaped fiber is measured to be 0.8 dB with a continuous laser. The nonlinear saturable absorption of D-shaped fiber SA is measured by a power-dependent transmission technique based on a balanced twin-detector measurement system, which has been elaborated in Ref. 24. The illumination pulse is delivered by a home-made passively mode-locked fiber laser (repetition rate: ~25 MHz, pulse duration: ~400 fs, central wavelength: ~1.55 μm). The power-dependent transmittance T is fitted by $T = A\exp[-\Delta T/(1 + I/I_{sat})]$[13,23], where A is the normalization constant, ΔT is the absolute modulation depth, I is the incident intensity, and I_{sat} is the saturation intensity. As shown in Fig. 2(b), the D-shaped fiber SA exhibits saturable absorption property that the transmittance increases with light intensity, and the modulation depth is measured as 0.95%. The saturable intensity is about 0.6 GW/cm^2, which is much larger than that of the graphene[5] or carbon nanotube[30].

The second SA is based on WS_2-PVA film, and the fabrication process can be described as follows. The as-prepared WS_2 solution is ultra-sonicated for 1-hour using a 300 W ultrasonic cleaner. Then, 5 wt% aqueous PVA solution and the WS_2 solution are mixed at the

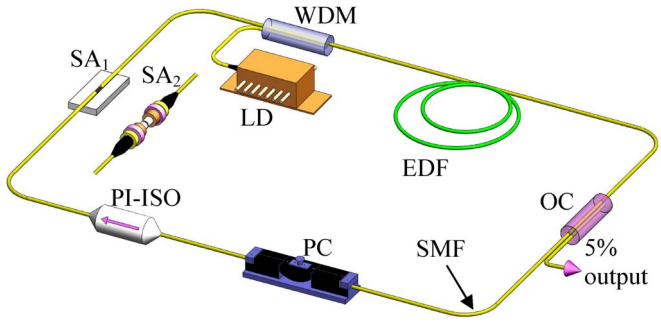

Figure 3 | Experimental setup of the fiber laser with WS_2 as a mode locker. LD: laser diode; WDM: wavelength division multiplexer; EDF: erbium-doped fiber; OC: optical coupler; SMF: single-mode fiber; PC: polarization controller; PI-ISO: polarization-independent isolator; SA_1: D-shaped fiber based SA; SA_2: PVA-film based SA.

volume ratio of 1 : 2 by a magnetic stirrer for 5 hours. The final mixture is dropped on a substrate. Slow evaporation under ambient temperature and pressure results in a PVA-composite film. The side profile and thickness of the film are shown in Fig. 1(f). Figure 2(c) shows the photograph of WS_2-PVA film that is coated on the facet of the fiber connector. In this case, the modulation depth and saturable power are given as about 1.8% and 0.75 GW/cm^2 by using the same measuring technique. Compared with dropping dispersions on a quartz plate[7] and optical deposition[8], the filmy polymer method would be more favorable to fabricate SA due to its superiority of low cost, flexibility, and controllability. During the experiment, we do not observe any other nonlinear response from fiber device or pure PVA film, indicating that the saturable absorption originates from WS_2 nanosheets alone.

Setup of WS_2 mode locked fiber laser. Fiber lasers exhibit inherent advantages of high gain coefficient, wide operating wavelength range, excellent heat dissipation, and robust mode confinement[31–35], and thus offer an attractive platform for testing the nonlinear absorption of the samples. The schematic diagram of the laser set up is shown in Fig. 3. Two WS_2-based SAs are used separately to realize passive mode locking of the fiber laser. The fiber resonator consists of a 3-m EDF (Nufen: EDFC-980-HP) with 3 dB/m absorption at 980 nm, a polarization-independent isolator, a wavelength-division multiplexer, a WS_2 SA, a polarization controller, and a fiber-based optical coupler with output ratio of 5%. The other fibers and pigtails of the components are SMFs with a total length of 20.2 m (19.9 m) for SA_1 (SA_2). The fiber laser is pumped by a 980 nm laser diode with the maximum power of 600 mW. The dispersion parameters D at 1.55 μm for EDF and SMF are −16 ps/(nm.km) and 17 ps/(nm.km), respectively. The net cavity dispersion β_2 is calculated as about −0.38 ps^2, and thus traditional soliton tends to be formed in the fiber laser.

Experimental observations. Continuous wave emission is achieved at an incident pump power of 10 mW using D-shaped fiber coated with WS_2 (SA_1). At appropriate pump power and polarization state, self-starting mode locking of fiber laser is achieved and shows clear hysteresis phenomenon[36]. For example, mode locking starts by increasing the pump power to 25 mW while vanishes by decreasing the pump power to 13 mW. A typical mode-locking state at 300 mW is shown in Fig. 4. The central wavelength and 3-dB bandwidth of the output spectrum are measured to be 1557 nm and 2.3 nm, respectively, as shown in Fig. 4(a). Several pairs of sidebands are symmetrically distributed at both sides of the spectrum, which are the typical characteristics of standard soliton pulses[37,38].

The auto-correlation trace of the output soliton is shown in Fig. 4(b), which has a full width at half maximum of about 2.1 ps. By using a sech^2 fitting, the pulse duration is given as 1.32 ps from the

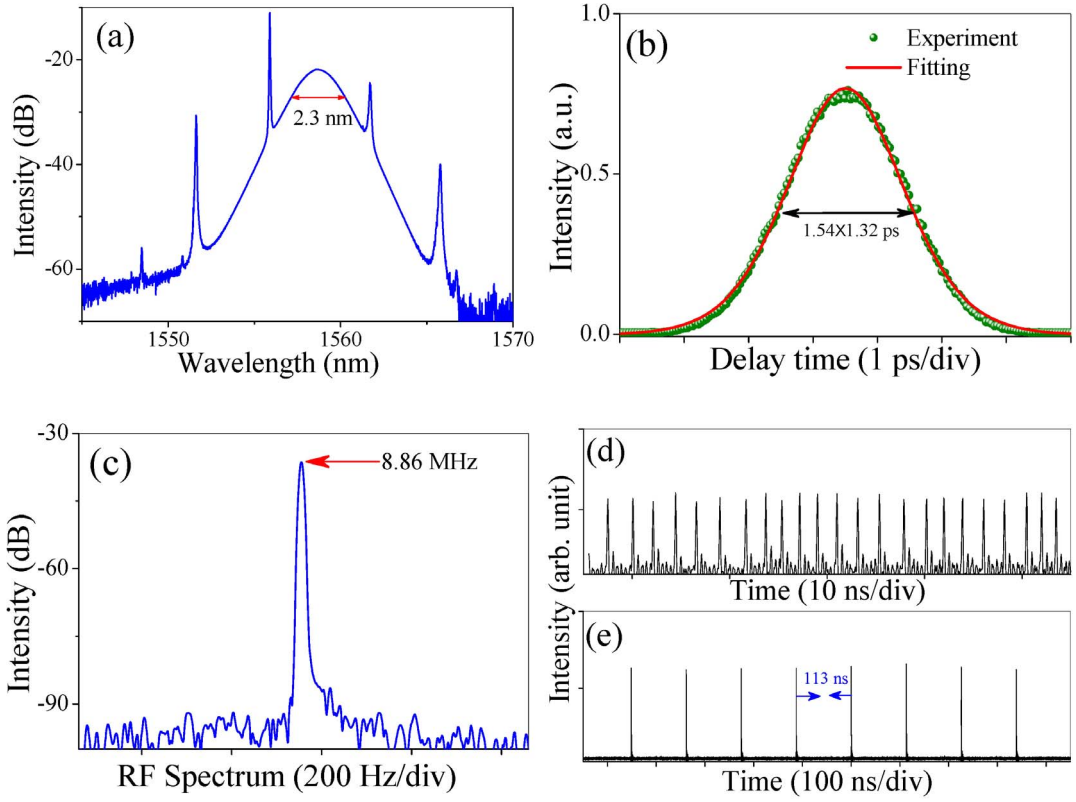

Figure 4 | (a) Spectrum, (b) auto-correlation trace, (c) RF spectrum, (d) pulse train at pump power of 300 mW, and (e) single-pulse mode locking at 15 mW. The SA is fabricated by depositing the WS_2 nanosheets onto D-shaped fiber.

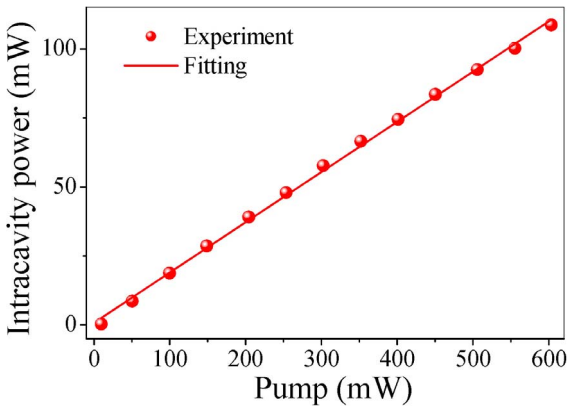

Figure 5 | Intracavity power of soliton mode locking as a function of pump power.

auto-correlation trace. The time bandwidth product is estimated to be 0.38, indicating that the output soliton is slightly chirped. Figure 4(c) illustrates the radio frequency (RF) spectrum at the span of 1 kHz and resolution of 9.1 Hz. The fundamental repetition rate is given as 8.86 MHz, which coincides with the cavity length of 23.2 m. The signal-to-noise ratio is higher than 50 dB, indicating its good mode-locking stability. Attributing to the peak power clamping effect of standard soliton[39], multiple pulses are formed in the fiber resonator, as demonstrated in Fig. 4(d). Noteworthily, stable single-pulse mode locking also can be achieved by decreasing the pump power to 15 mW, as shown in Fig. 4(e). The interval between adjacent pulses is measured as 113 ns, which is equal to the cavity round-trip time.

An inherent feature of the proposed SA is the ultra-high optical damage threshold. During the experiment, mode locking can be always observed when the pump power ranges from the self-starting threshold value to the maximum available pump power. Figure 5 shows the intracavity power as a function of pump power at the mode-locking state. One can observe that the intracavity power almost increases linearly with the pump. By using a linear fitting, the slope efficiency is given as 0.184. At the maximum pump power of 600 mW, there are 50 pulses co-propagating in the fiber laser. Considering the repetition of 8.86 MHz and average power of 110 mW, the energy per pulse is calculated as 0.248 nJ. The WS_2-based SA may benefit the applications in fields of high-power pulsed laser, harmonic mode locking, materials processing, and so on.

Slightly tuning the polarization controller, the other operation state also can be obtained in the fiber laser. Figure 6 shows the typical operation sate at a pump power of 600 mW. The output spectrum exhibits a triangular profile with the bandwidth of 0.6 nm, as shown in Fig. 6(a). The temporal profile is illustrated in Fig. 6(b), in which the interval between adjacent pulses is equal to the cavity round trip (113 ns). As shown in the inset of Fig. 6(b), the pulse pocket consists of numerous pulses with randomly distributed intensities and phases, similar with noiselike pulse reported in previous works[40,41].

Utilizing WS_2-PVA film (SA_2), stable soliton mode locking is also observed at pump of 190 mW in the same fiber laser. At the maximum pump power of 600 mW, mode locking operation can be maintained for several hours as long as the experiment condition keeps unchanged. Figures 7(a) and 7(b) show the spectrum and auto-correlation trace of the pulse at the pump power of 450 mW, respectively. Here, the 3-dB spectral width and pulse duration are given as 3.1 and 1.2 ps, respectively. The corresponding time bandwidth product is calculated as 0.34, suggesting that the output soliton is slightly chirped. The fundamental repetition rate is given as 8.96 MHz, as shown in the inset of Fig. 7(a). The oscilloscope trace in the inset of Fig. 7(b) indicates that multiple pulses are formed in the fiber resonator, which is similar with that of Fig. 4(d).

It is worth to note that mode locking operation can be easily established when the D-shaped fiber is coated with WS_2 while vanishes when the D-shaped fiber is coated with pure-PVA, air, water, alcohol, or the mixture of water with alcohol. Additionally, we have purposely removed the WS_2-PVA film from the laser cavity to verify whether the soliton formation is purely caused by WS_2. In this case, no mode locking is observed, despite that the pump power is changed from zero to the maximum (600 mW) and polarization controller is tuned over a full range. By inserting the WS_2-PVA film into fiber laser, mode locking operation can be obtained again. As a result, we conclude that the mode locking operation is purely induced by WS_2 rather than other components. Based on experimental observations, we believe that WS_2 nanosheets exhibit nonlinear saturable absorption property and are able to serve as mode locker for ultrafast fiber lasers.

Discussion

The mechanism of saturable absorption in semiconductor can be described by a two-level model[13]. When semiconductor is excited by light with photon energy larger than the gap energy, electrons will be transferred from the valance band to the conduction band. Under strong excitation, electrons from the valence band are excited into the conduction band and the states in the valence band become depleted, while the finial states in the conduction band are partially occupied. Further excitation from the valence band is blocked and no absorption is induced, leading to a saturable absorption condition that low-intensity (high-intensity) light experiences large (small) loss. As a result, it is easy to understand that topological insulator and MoS_2 exhibit nonlinear saturable absorption property for light with photon energy larger than the gap energy.

The direct bandgap of monolayer MoS_2 is about 1.8 eV (0.688 μm) and the indirect gap of the bulk material is in the range of 0.86–

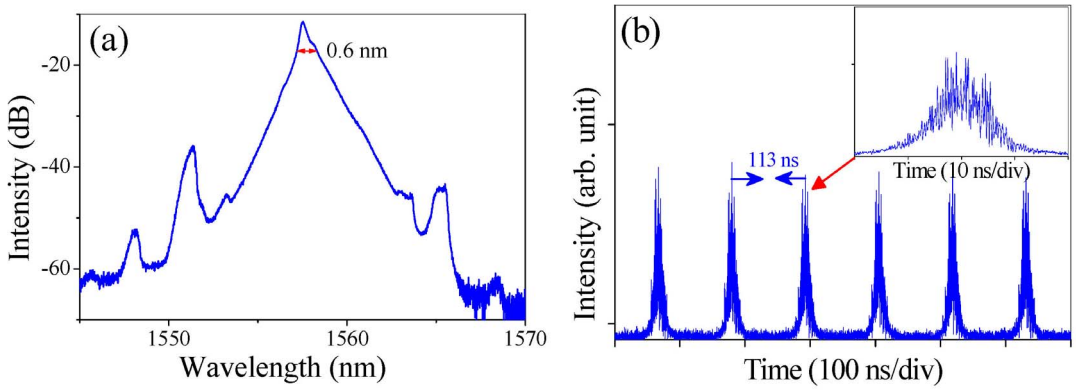

Figure 6 | (a) Spectrum and (b) pulse train of noiselike pulse operation. The inset shows a zoom-in image of the output pulses.

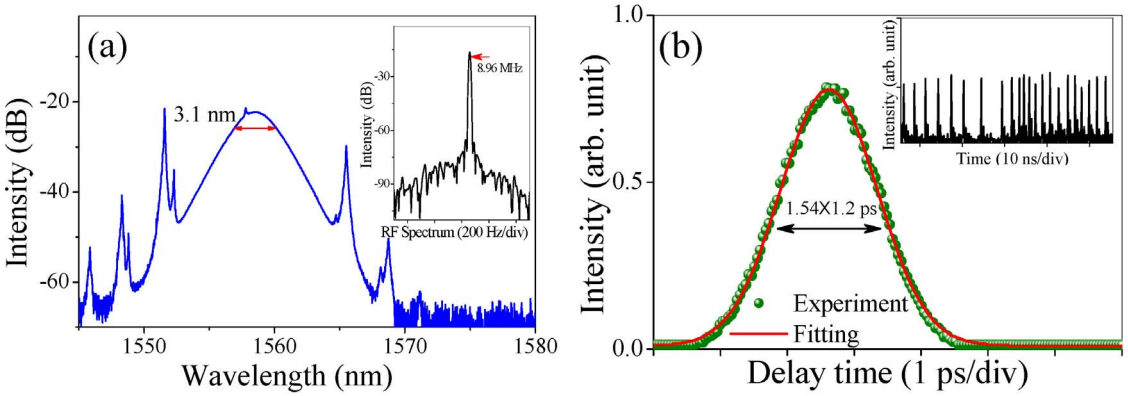

Figure 7 | (a) Spectrum and (b) auto-correlation trace of mode-locked pulses at pump power of 450 mW. The insets in Figs. 7(a) and (b) show the RF spectrum and oscilloscope trace. The SA is based on WS_2-PVA film.

1.29 eV (1.44–0.96 μm)[23]. It seems that MoS_2 nanosheets are beyond the application as a saturable absorption device for laser wavelength larger than 1.44 μm[14]. However, experimental results have revealed that MoS_2 exhibits saturable absorption property at 0.4, 0.8, 1.06, 1.42, 1.55, and 2.1 μm[22–27,42]. Various theories have been proposed to interpret the intriguing experimental observations, such as defect-induced bandgap decreasing[23,43,44] as well as coexistence of semiconducting and metallic states[24]. Like MoS_2, our experiment demonstrates that WS_2 exhibits saturable absorption property at 1.55 μm, in which the energy per photon (0.8 ev) is lower than the direct bandgap of monolayer WS_2 (2 ev)[45] or indirect gap of the bulk WS_2 (1.34 ev)[46]. Until now the nonlinear saturable absorption mechanism of WS_2 nanosheets has not been clearly raveled at such waveband. As MoS_2 and WS_2 possess similar lattice structures and photonic properties[15,17,21], one could infer that saturable absorption mechanism of WS_2 may be similar with that of the MoS_2 reported previously[23,24,42].

Methods

Measurement method. An optical spectrum analyzer (Yokogawa AQ6370), a commercial autocorrelator (APE Pulse Check), a RF analyzer, and a digital oscilloscope are employed to characterize the laser output simultaneously.

1. Novoselov, K. S. *et al.* Two-dimensional gas of massless Dirac fermions in graphene. *Nature* **438**, 197–200 (2005).
2. Gan, X. *et al.* Chip-integrated ultrafast graphene photodetector with high responsivity. *Nat. Photonics* **7**, 883–887 (2013).
3. Grigorenko, A. N., Polini, M. & Novoselov, K. S. Graphene plasmonics. *Nat. photonics* **6**, 749–758 (2012).
4. Zhang, H. *et al.* Large energy soliton erbium-doped fiber laser with a graphene-polymer composite mode locker. *Appl. Phys. Lett.* **95**, 141103 (2009).
5. Sun, Z. *et al.* Graphene mode-locked ultrafast laser. *ACS Nano* **4**, 803–810 (2010).
6. Zhang, H. *et al.* Topological insulators in Bi_2Se_3, Bi_2Te_3 and Sb_2Te_3 with a single Dirac cone on the surface. *Nat. Phys.* **5**, 438–442 (2009).
7. Zhao, C. *et al.* Ultra-short pulse generation by a topological insulator based saturable absorber. *Appl. Phys. Lett.* **101**, 211106 (2012).
8. Luo, Z. C. *et al.* 2 GHz passively harmonic mode-locked fiber laser by a microfiber-based topological insulator saturable absorber. *Opt. Lett.* **38**, 5212–5215 (2013).
9. Radisavljevic, B., Radenovic, A., Brivio, J., Giacometti, V. & Kis, A. Single-layer MoS_2 transistors. *Nat. Nanotech.* **6**, 147–150 (2011).
10. Berkdemir, A. *et al.* Identification of individual and few layers of WS_2 using Raman Spectroscopy. *Sci. Rep.* **3**, 1755 (2013).
11. Popa, D. *et al.* Sub 200 fs pulse generation from a graphene mode-locked fiber laser. *Appl. Phys. Lett.* **97**, 203106 (2010).
12. Liu, J., Wu, S., Yang, Q. H. & Wang, P. Stable nanosecond pulse generation from a graphene-based passively Q-switched Yb-doped fiber laser. *Opt. Lett.* **36**, 4008–4010 (2011).
13. Yu, H. *et al.* Topological insulator as an optical modulator for pulsed solid-state lasers. *Laser Photon. Rev.* **7**, 77–83 (2013).
14. Bonaccorso, F. & Sun, Z. P. Solution processing of graphene, topological insulators and other 2d crystals for ultrafast photonics. *Opt. Mater. Express* **4**, 63–78 (2014).
15. Ramakrishna Matte, H. *et al.* MoS_2 and WS_2 analogues of graphene. *Angew. Chem.* **122**, 4153–4156 (2010).
16. Li, H., Wu, J., Yin, Z. & Zhang, H. Preparation and applications of mechanically exfoliated single-layer and multilayer MoS_2 and WSe_2 nanosheets. *Acc. Chem. Res.* **47**, 1067–1075 (2014).
17. Coleman, J. N. *et al.* Two-dimensional nanosheets produced by liquid exfoliation of layered materials. *Science* **331**, 568–571 (2011).
18. Liu, Y. *et al.* Preparation, characterization and photoelectrochemical property of ultrathin MoS_2 nanosheets via hydrothermal intercalation and exfoliation route. *J. Alloys Compd.* **571**, 37–42 (2013).
19. Lee, Y. *et al.* Synthesis of large-area MoS_2 atomic layers with chemical vapor deposition. *Adv. Mater.* **24**, 2320–2325 (2012).
20. Zheng, J. *et al.* High yield exfoliation of two-dimensional chalcogenides using sodium naphthalenide. *Nat. Commun.* **5**, 2995 (2014).
21. Molina-Sanchez, A. & Wirtz, L. Phonons in single-layer and few-layer MoS_2 and WS_2. *Phys. Rev. B* **84**, 155413 (2011).
22. Wang, K. *et al.* Ultrafast saturable absorption of two-dimensional MoS_2 nanosheets. *ACS Nano* **7**, 9260–9267 (2013).
23. Wang, S. *et al.* Broadband few-layer MoS_2 saturable absorbers. *Adv. Mater.* **26**, 3538–3544 (2014).
24. Zhang, H. *et al.* Molybdenum disulfide (MoS_2) as a broadband saturable absorber for ultra-fast photonics. *Opt. Express* **22**, 7249–7260 (2014).
25. Liu, H. *et al.* Femtosecond pulse erbium-doped fiber laser by a few-layer MoS_2 saturable absorber. *Opt. Lett.* **39**, 4591–4594 (2014).
26. Xia, H. *et al.* Ultrafast erbium-doped fiber laser mode-locked by a CVD-grown molybdenum disulfide (MoS_2) saturable absorber. *Opt. Express* **22**, 17341–17348 (2014).
27. Khazaeizhad, R. *et al.* Mode-locking of Er-doped fiber laser using a multilayer MoS_2 thin film as a saturable absorber in both anomalous and normal dispersion regimes. *Opt. Express* **22**, 23732–23742 (2014).
28. Néstor, P. *et al.* Photosensor device based on few-layered WS_2 films. *Adv. Funct. Mater.* **23**, 5511–5517 (2013).
29. Song, Y., Yamashita, S., Goh, C. S. & Set, S. Y. Carbon nanotube mode lockers with enhanced nonlinearity via evanescent field interaction in D-shaped fibers. *Opt. Lett.* **32**, 148–150 (2007).
30. Liu, X. *et al.* Versatile multi-wavelength ultrafast fiber laser mode-locked by carbon nanotubes. *Sci. Rep.* **3**, 2718 (2013).
31. Lecaplain, C., Grelu, P., Soto-Crespo, J. M. & Akhmediev, N. Dissipative rogue waves generated by chaotic pulse bunching in a mode-locked laser. *Phys. Rev. Lett.* **108**, 233901 (2012).
32. Tsatourian, V. *et al.* Polarization dynamics of vector soliton molecules in mode locked fibre laser. *Sci. Rep.* **3**, 3154 (2013).
33. Mao, D. *et al.* Flexible high-repetition-rate ultrafast fiber laser. *Sci. Rep.* **3**, 3233 (2013).
34. Oktem, B., Ülgüdür, C. & Ilday, F. Ö. Soliton-similariton fibre laser. *Nat. Photonics* **4**, 307–311 (2010).
35. Dudley, J. M., Finot, C., Richardson, D. J. & Millot, G. Self-similarity in ultrafast nonlinear optics. *Nat. Physics* **3**, 597–603 (2007).
36. Liu, X. Hysteresis phenomena and multipulse formation of a dissipative system in a passively mode-locked fiber laser. *Phys. Rev. A* **82**, 023811 (2010).
37. Nelson, L. E., Jones, D. J., Tamura, K., Haus, H. A. & Ippen, E. P. Ultrashort-pulse fiber ring lasers. *Appl. Phys. B* **65**, 277–294 (1997).
38. Liu, X. M. Soliton formation and evolution in passively mode-locked lasers with ultralong anomalous-dispersion fibers. *Phys. Rev. A* **84**, 023835 (2011).
39. Tang, D. Y., Zhao, L. M., Zhao, B. & Liu, A. Q. Mechanism of multisoliton formation and soliton energy quantization in passively mode-locked fiber lasers. *Phys. Rev. A* **72**, 043816 (2005).
40. Kobtsev, S., Kukarin, S. & Fedotov, Yu. Ultra-low repetition rate mode-locked fiber laser with high energy pulses. *Opt. Express* **16**, 21936–21941 (2008).
41. Horowitz, M., Barad, Y. & Silberberg, Y. Noiselike pulses with a broadband spectrum generated from an erbium-doped fiber laser. *Opt. Lett.* **22**, 799–801 (1997).

42. Wang, K. *et al.* Broadband ultrafast nonlinear absorption and nonlinear refraction of layered molybdenum dichalcogenide semiconductors. *Nanoscale* **6**, 10530–10535 (2014).
43. Zheng, L. *et al.* Identification of active atomic defects in a monolayered tungsten disulphide nanoribbon. *Nat. Commun.* **2**, 213 (2011).
44. Qiu, H. *et al.* Hopping transport through defect-induced localized states in molybdenum disulphide. *Nat. Commun.* **4**, 2642 (2013).
45. Zhao, W. *et al.* Evolution of electronic structure in atomically thin sheets of WS_2 and WSe_2. *ACS Nano* **7**, 791–797 (2012).
46. Klein, A., Tiefenbacher, S., Eyert, V., Pettenkofer, C. & Jaegermann, W. Electronic band structure of single-crystal and single-layer WS_2: Influence of interlayer van der Waals interactions. *Phys. Rev. B* **64**, 205416 (2001).

Acknowledgments

This work was supported by the National Natural Science Foundation of China (Grants Nos. 61405161, 11404263, 61377035, 61176085, 61377055), the 973 Program (Grant No. 2012CB921900), Fundamental Research Funds for the Central Universities (Grant Nos. 3102014JCQ01101, 3102014JCQ01099, 3102014JCQ01085), and financial support from the Department of Education of Guangdong Province (Grant No. gjhz1103).

Author contributions

D.M. designed the work, performed the experiments, and wrote the paper. Y.W. and S.H. fabricated and tested the D-shaped fiber. C.M. measured the property of WS_2 nanosheets. L.H. performed the part of experiment. B.J. and X.G. carried out the data analysis and revised the manuscript. W.Z., T.M. and J.Z. contributed to the scientific discussion and considerably improved the manuscript presentation. All authors discussed the results and substantially contributed to the manuscript.

Additional information

Competing financial interests: The authors declare no competing financial interests.

How to cite this article: Mao, D. *et al.* WS_2 mode-locked ultrafast fiber laser. *Sci. Rep.* **5**, 7965; DOI:10.1038/srep07965 (2015).